Coexisting structures in ^{105}Ru

S. Lalkovski,[1,*] D. Ivanova,[1] E. A. Stefanova,[2] A. Korichi,[3] P. Petkov,[2] J. Kownacki,[4] T. Kutsarova,[2] A. Minkova,[1] D. Bazzacco,[5] M. Bergström,[6] A. Görgen,[7,†] B. Herskind,[6] H. Hübel,[7] A. Jansen,[7] S. Kisyov,[1] T. L. Khoo,[8] F. G. Kondev,[9] A. Lopez-Martens,[2] Zs. Podolyák,[10,‡] G. Schönwasser,[7] and O. Yordanov[2]

[1]*Faculty of Physics, University of Sofia, Sofia 1164, Bulgaria*

[2]*Institute for Nuclear Research and Nuclear Energy, Bulgarian Academy of Science, Sofia 1784, Bulgaria*

[3]*CSNSM Orsay, IN2P3/CNRS, F-91405, France*

[4]*Heavy-Ion Laboratory, University of Warsaw, ul. "Pasteura" 5A, 02-093 Warzsawa, Poland*

[5]*INFN, Sezione di Padova, I-35131 Padova, Italy*

[6]*The Niels Bohr Institut, Blegdamsvej 17, DK-2100 Copenhagen, Denmark*

[7]*Helmholtz-Institut für Strahlen- und Kernphysik, Universität Bonn, Nussallee 14-16, D-53115 Bonn, Germany*

[8]*Physics Division, Argonne National Laboratory, Argonne, Illinois 60439, USA*

[9]*Nuclear Engineering Division, Argonne National Laboratory, Argonne, Illinois 60439, USA*

[10]*INFN, Laboratori Nazionali di Legnaro, I-35020 Padova, Italy*

(Received 19 March 2014; published 18 June 2014)

New positive-parity states, having a bandlike structure, were observed in ^{105}Ru. The nucleus was produced in an induced fission reaction, and the prompt γ-rays, emitted from the fragments, were detected by the EUROBALL III multidetector array. The partial scheme of excited ^{105}Ru levels is analyzed within the triaxial-rotor-plus-particle approach.

DOI: 10.1103/PhysRevC.89.064312 PACS number(s): 21.10.Re, 21.60.Ev, 23.20.Lv, 27.60.+j

I. INTRODUCTION

^{105}Ru is located on the Segré chart between its heaviest stable isotope ^{104}Ru [1] and the most exotic ^{117,118,119}Ru nuclei, produced in relativistic fission [2–4]. Being just on the edge of the line of β stability, only a few experimental methods can be used to populate its excited states. So far, the nucleus has been studied in ^{105}Tc β decay [5], in the ^{104}Ru(d,p) reaction [6,7], and in n capture on ^{104}Ru [8,9]. However, these reaction mechanisms are highly selective and populate only low-spin states. In the 1990s high-resolution, high-granularity multidetector γ-ray arrays became available, which have enabled the use of induced fission reactions for γ-ray spectroscopy, providing the opportunity to fill in the gap of transitional nuclei situated between the line of beta stability and the most exotic neutron-rich nuclei produced in fission. By using an induced fission reaction, the intruder negative-parity band in ^{105}Ru was observed for the first time and extended to $(31/2^-)$ [10]. The present work reports on new results for ^{105}Ru, obtained also from induced fission. Two positive-parity bands were observed on top of the known $7/2^+_1$ and $5/2^+_2$ states, which help to parametrize the rigid-triaxial-rotor-plus-particle model and test its applicability to the low-lying low-spin states observed prior to our study in ^{105}Ru.

II. EXPERIMENT AND DATA ANALYSIS

^{105}Ru was produced as a fission fragment in the disintegration of the $^{198}_{82}$Pb compound nucleus, which was synthesized in the $^{30}_{14}$Si + $^{168}_{68}$Er reaction at a beam energy of $E(^{30}\text{Si}) = 142$ MeV. In order to stop the recoils, the 1.15 mg/cm^2 thick ^{168}Er target was deposited on a 9 mg/cm^2 gold backing. The γ rays, emitted by the fission products, were detected by the EUROBALL III multidetector array comprising 30 single high-purity germanium (HPGe) detectors, 26 clover detectors, and 15 cluster detectors with anti-Compton shields. The acquisition system was triggered by triple γ-γ-γ coincidences. Three dimensional (3D) cubes were sorted and analyzed with the RADWARE software [11]. The extended level scheme of $^{194}_{82}$Pb, produced in the $4n$ fusion-evaporation channel, was previously reported in Ref. [12]. Data for $^{98,100,102}_{42}$Mo and $^{109,111}_{46}$Pd nuclei, produced in the same experiment as fission fragments, are published in Refs. [13] and [14]. Their respective complementary $_{40}$Zr and $_{36}$Kr fragments were found in the $4n$–$6n$ fusion-fission channels.

Sample energy spectra, obtained from the present experiment, are shown in Fig. 1, and the partial level scheme of ^{105}Ru, based on the coincidence measurements, is present in Fig. 2.

In the present experiment, the complementary fragments to $^{105}_{44}$Ru are $_{38}$Sr nuclei, given that no proton evaporation can occur in the induced fission reactions. In order to identify its most probable complementary Sr isotopes, prompt transitions with energies of 365, 569, 725, and 843 keV from the negative-parity band in ^{105}Ru [10] were used. Figure 1(a) shows a sample γ-ray spectrum in coincidence with the 365- and 569-keV transitions. The 2079- and 1309-keV transitions in ^{89}Sr [15], and the 1836- and 898-keV transitions in ^{88}Sr [16], which correspond to the $4n$ and $5n$ fission-fission channels, respectively, were observed in coincidence with the ^{105}Ru negative-parity band members. The ^{88,89}Sr being complementary fragments to ^{105}Ru is consistent with the number of neutrons, evaporated prior to the γ-ray emission, observed

*stl@phys.uni-sofia.bg

†Present address: DAPNIA/SPhN, CEA-Saclay, Gif-sur-Yvette, France.

‡Present address: Department of Physics, University of Surrey, Guildford GU27XH, UK.

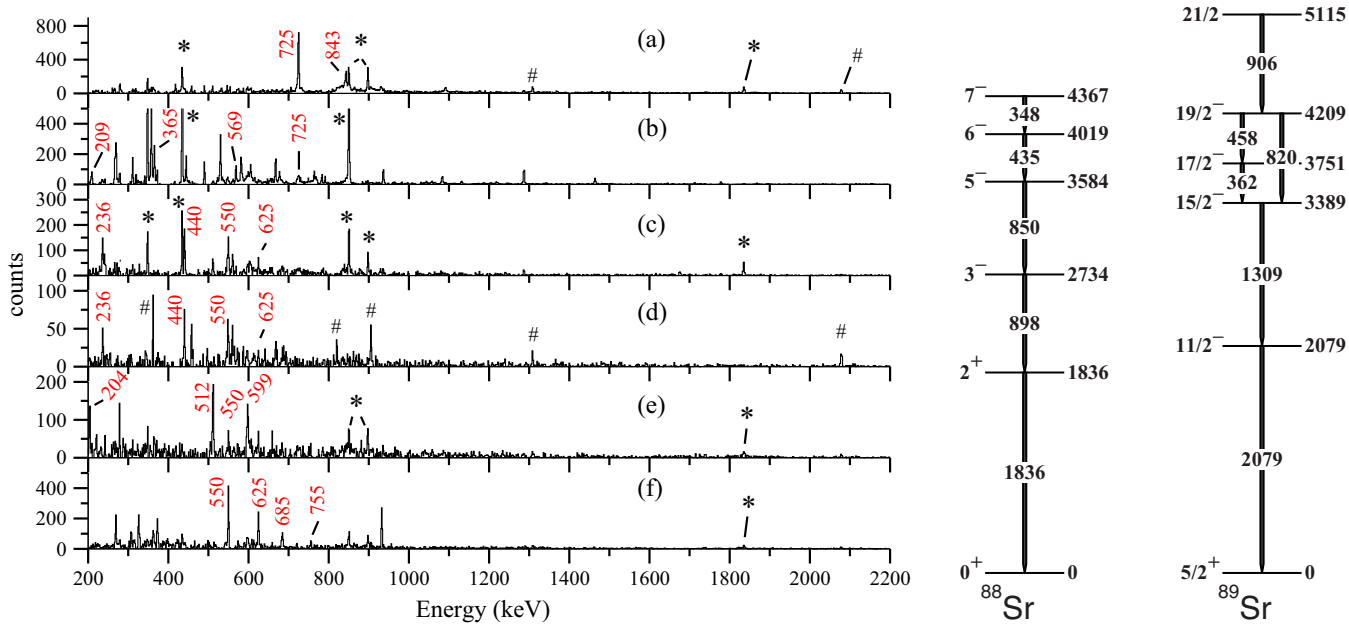

FIG. 1. (Color online) Left-hand side: γ-ray spectra, gated on (a) 365- and 569-keV transitions; (b) 1836- and 898-keV transitions; (c) 209- and 1836- or 209- and 898-keV transitions; (d) 209- and 2079-keV or 209- and 1309-keV transitions; (e) 209- and 235-keV transitions; (f) 209- and 440-keV transitions. The γ lines belonging to the ^{88}Sr level scheme are denoted with a star symbol *. The γ lines belonging to the ^{89}Sr level scheme are denoted with the hash symbol #. Right-hand side: Partial level schemes of ^{88}Sr and ^{89}Sr according to Refs. [16] and [15].

in the cases of ^{109,111}Pd [14] and ^{98,100,102}Mo fragments [13]. The partial level schemes of ^{88,89}Sr are shown in Fig. 1.

To search for the positive-parity yrast states in ^{105}Ru, coincidence spectra gated on the 1309- and 2079-keV transitions in ^{89}Sr and 898- and 1836-keV in ^{88}Sr were simultaneously studied. A sample spectrum, gated on the 1836- and 898-keV transitions in ^{88}Sr, is shown in Fig. 1(b). A weak 209-keV transition was observed both in the ^{88}Sr and ^{89}Sr gated spectra, which suggests that it is in a complementary Ru nucleus. Indeed, this transition deexcites the $7/2^+_1$ state in ^{105}Ru, produced in (n,γ) [8,9] and β decay [5]. There, the 209-keV transition is the strongest decay branch from the 230-keV $7/2^+_1$ level. Further, cross-coincidence gates, imposed on the 209-keV transition and transitions in the complementary ^{88}Sr and ^{89}Sr nuclei, reveal that the 209-keV transition is in coincidence with transitions of 440 and 550 keV. Sample spectra are shown in Figs. 1(c) and 1(d). Spectra, gated on the 209- and 440- or 550-keV transitions show they are part of the band extended up to 3285 keV in Fig. 2. In the present data, the 230-keV level decays also by a second branch of weak transitions with energies of 121 and 108 keV, which were also observed in the (n,γ) [8,9] and β-decay [5] data, confirming that the band is a part of the ^{105}Ru level scheme.

Two more transitions with energies of 204 and 235 keV were observed in coincidence with the 550- and 625-keV γ rays. The last two spectra in Figs. 1(e) and 1(f) show that the 209- and 235-keV transitions link the band based on the $7/2^+$ state to a second sequence of transitions on top of the second $5/2^+$ state at 108 keV.

The γ-ray energies (E_γ) and their relative intensities (I_γ), observed in the present study, are listed in Table I along with the γ-ray energies ($E_\gamma^{\rm ENS}$) and ($I_\gamma^{\rm ENS}$), adopted in Ref. [17]. The intensities I_γ are normalized with respect to the intensity of the 550.1-keV transition, while the $I_\gamma^{\rm ENS}$, from the gammas adopted in ENSDF, are normalized with respect to the intensity of the strongest decay branch to each level. Due to the poor statistics, no I_γ were obtained for the 108.4-, 121.1-, and 229.8-keV transitions. For the purpose of the discussion below, the branching ratios from the adopted gammas will be used in these cases.

The spin and parity (J^π) assignments to the states, below the 230-keV level, are based on the β-decay feeding [5], on the decay branches of primary transitions observed from the n-capture state at 5.9 MeV [8,9], on the L transfer in (d,p) reaction [6,7], on and the γ-decay pattern to states with known spins and parities. The J^π assignments to the higher-energy states are based on the observed band structure, and for each level on the γ-decay branches to states with known spin and parity assignments. The J^π assignments in the present work are also supported by the systematics of the positive-parity states in the Ru isotopic chain. Only $M1$ and $E2$ nature is assumed for the prompt γ rays above the $7/2^+_1$ state. Given that the induced fission reaction populates mainly yrast states, it can be expected that at moderate and high energies there will be a little overlap between the states produced in the present experiment and in the β-decay or n-capture primary transitions.

By applying the above procedures, two of the J^π assignments, made in the present work, differ significantly from the $J^{\pi,\rm ENS}$ values adopted in Ref. [17]. Thus, for example a 466-keV level is reported from β-decay, ^{104}Ru(d,p), and ^{104}Ru(n,γ) data. There, the level decays via a branch of four transitions with energies of 307, 358, 446, and 466 keV to levels with $J^\pi = 1/2^+$, $3/2^+$, and $5/2^+$. Also, the 466-keV level is fed by a primary transition from the $1/2^+$ n-capture

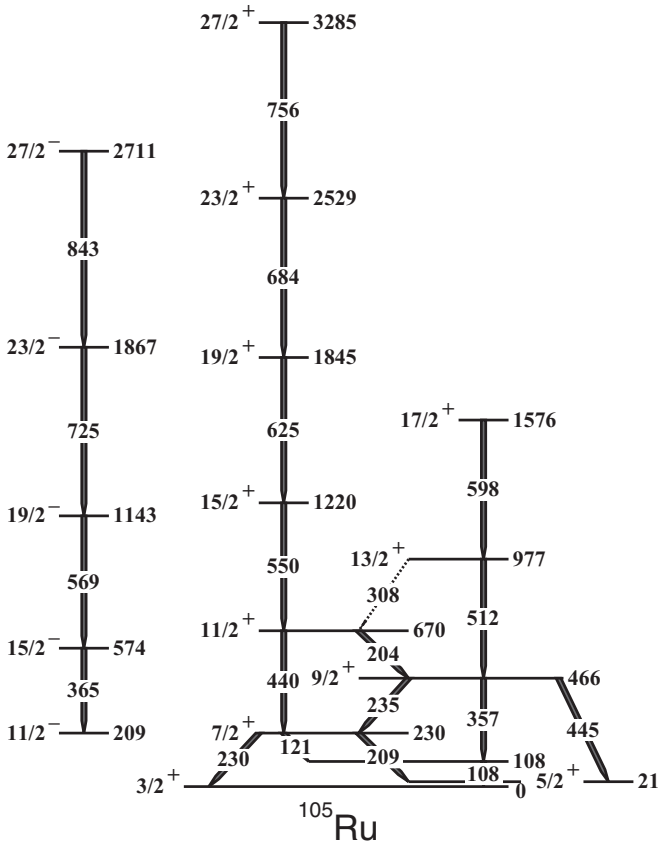

FIG. 2. Partial level scheme of ^{105}Ru as observed in the present study. Level and γ-ray energies are rounded values from Table I. Spin and parity assignments to the levels, observed in the present work, are only tentative. Arguments for these assignments are given in the text.

state at 5.9 MeV which constrains the possible J^π assignments to $J^\pi = 1/2^+$ and $3/2^+$, with the last one being adopted in Ref. [17]. In contrast, the 466-keV level, observed in the present study, decays via a strong 235-keV transition in addition to the main 357-keV decay branch, and the 307- and 466-keV decay branches were not observed at all. Therefore the state observed in the present study is tentatively interpreted as a $J^\pi = 9/2^+$ state, different from the low-spin 466-keV level known prior to our work.

A similar situation occurs for the 670-keV level, which is observed to decay via 204- and 440-keV transitions in the present study, while in Ref. [17] the level at 670 keV is deexcited by 398- and 563-keV transitions. Again, the low-spin assignment to the 670-keV level in NNDC is based on the feeding from the n-capture state at 5.9 MeV via a 5.24-MeV primary transition. In contrast to the NNDC data, the 670-keV level in the present study decays to the $7/2^+$ and $9/2^+$ states which, along with the assumption that it is an yrast state, leads to $J^\pi = 11/2^+$ assignment to this level.

Before closing this section, we should note that the intensity balance at the 21-keV level, performed from the n-capture data [9], leads to an experimental electron conversion coefficient $\alpha_{\rm exp} \leqslant 25.2$, which along with the electron conversion coefficients calculated for a pure $M1$ or $E2$ 20.56-keV transition, $\alpha_{M1} = 4.016$ and $\alpha_{E2} = 409.4$ [18], respectively, gives a multipole mixing ratio $\delta \leqslant 0.23$. The half-life $T_{1/2} = 340(15)$ ns of the first excited state was measured by the $143.25\gamma - 20.55\gamma(t)$ delayed coincidences in the ^{105}Tc β decay [5], which leads to a hindered $M1$ component with $B(M1) = 2.7 \times 10^{-4}$ W.u. and possibly enhanced $E2$ component with $B(E2) \leqslant 30.7$ W.u.

TABLE I. Gamma-decay properties: initial level energy E_i in (keV), obtained from a least-squares fit to the γ-ray energies E_γ, observed in the present work; spin/parity assignments J_i^π to the levels in ^{105}Ru; γ-ray energies E_γ in (keV) and relative intensities I_γ, normalized with respect to the intensity of the 550-keV transition. The $J^{\pi,\rm ENS}$ assignments, γ-ray energies $E_\gamma^{\rm ENS}$ and intensities $I_\gamma^{\rm ENS}$, adopted by NNDC [17], are also listed for completeness. The level energies, adopted by NNDC [17], deviate by less then one keV from E_i and hence are not given in a separate column.

E_i	J_i^π	E_γ	I_γ	$J^{\pi,\rm ENS}$	$E_\gamma^{\rm ENS}$	$I_\gamma^{\rm ENS}$
20.9(11)	$5/2^+$			$5/2^+$	20.559	100
108.4(8)	$5/2^+$			$5/2^+$	87.40	<1.1
		108.4			107.945	100
229.8(8)	7/2+	121.2		$7/2^+$	121.49	16(4)
		208.6	76(8)		208.89	100
		229.8			229.51	16(4)
465.7(10)	(9/2+)	235.4	68(6)	$(3/2)^+$	306.76	55(20)
		357.3	76(8)		358.15	100
		445.1	⩽12		445.81	71(8)
					466.23	66(6)
670.1(11)	$(11/2^+)$	204.3	28(3)	$\leqslant 5/2^+$	397.8	8(4)
		440.4	104(9)		562.7	100
977.4(14)	$(13/2^+)$	511.7	42(5)			
1220.2(15)	$(15/2^+)$	550.1	100			
1575.6(17)	$(17/2^+)$	598.2	⩽40			
1845.1(18)	$(19/2^+)$	624.9	68(3)			
2529.3(21)	$(23/2^+)$	684.2	29.6(15)			
3285.4(23)	$(27/2^+)$	756.1	13.8(11)			

The 164-keV level in Ref. [17], not observed in the present study, decays with $T_{1/2} = 55(7)$ ns via a week 55-keV transition to the 108-keV $J^\pi = 5/2_2^+$ level as well as via a strong 143-keV $M1 + E2$ transition to the 21-keV $5/2_1^+$ level. In Ref. [17], $J^\pi = 3/2^+,5/2^+$ was assigned to this level. Hence, the reduced transition probabilities are $B(M1;55\gamma) = 1.01 \times 10^{-4}$ (22) W.u. and $B(M1;143\gamma) = 1.00 \times 10^{-4}$ (15) W.u. for the two decay branches, respectively. The respective $E2$ component of the 143-keV transition has $B(E2;143\gamma) = 0.27$ (13) W.u. Thus, the two low-lying isomeric states, observed in ^{105}Ru prior our study, decay via hindered $M1$ transitions.

III. DISCUSSION

Even though the low-lying states in ^{105}Ru are extensively studied via different experiments, their structure is still not well understood. Thus, from (d,p) reactions [6,7], large spectroscopic factors were obtained for the $J^\pi = 5/2_1^+$ (21 keV), $1/2_1^+$ (160 keV), $11/2_1^-$ (209 keV), $7/2_1^+$ (230 keV), and $3/2_2^+$ (466 keV) states in ^{105}Ru, shown in the experimental level scheme on Fig. 3, suggesting that they contain a large fraction

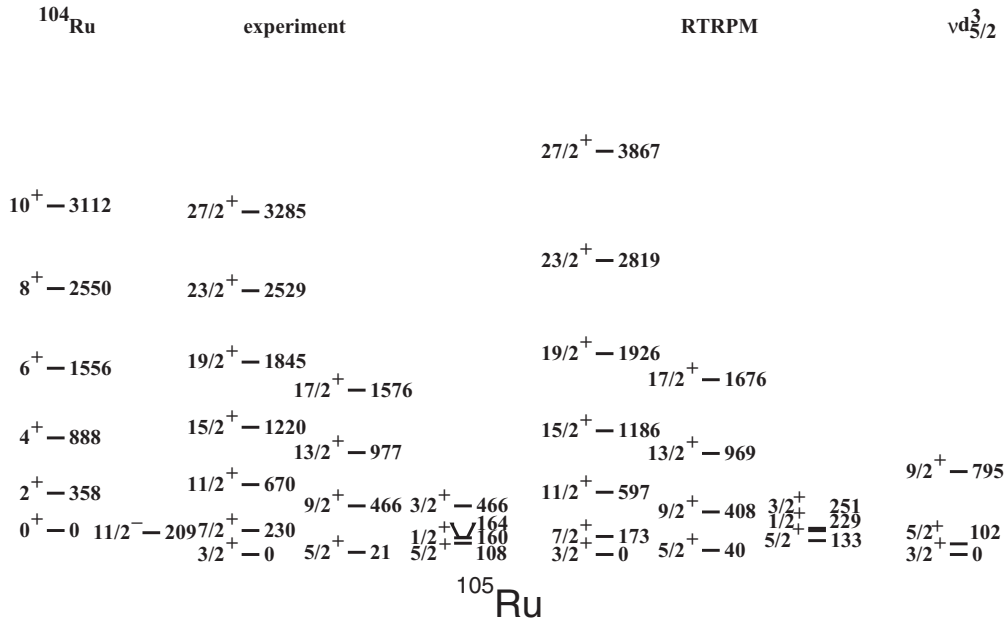

FIG. 3. Experimental and theoretical ^{105}Ru level schemes. The $\epsilon_2 = 0.24$, $\epsilon_4 = -0.013$, $\gamma = 20^\circ$, and $E_{2^+} = 0.2$ MeV parameters were used to obtain the rigid-triaxial-rotor-plus-particle model (RTRPM) spectrum. The empirical shell-model calculations within the $\nu d_{5/2}^3$ coupling scheme are parametrized with respect to the ^{104}Ru data.

of the single-particle strength of the $\nu 2d_{5/2}$, $\nu 3s_{1/2}$, $\nu 1h_{11/2}$, $\nu 1g_{7/2}$, and $\nu 2d_{3/2}$ orbitals. However, ^{105}Ru has a high level density at low energies [17] and the remaining single-particle strength is distributed over a larger number of states. In the shell-model approach, some of these states can be interpreted as seniority $v = 3$ states [19]. Such an interpretation was already suggested in [8] for the ground state, in order to account for the small spectroscopic factor observed in the (d, p) reaction. Indeed, $(\nu d_{5/2})^3$ calculations, shown in Fig. 3, with a two-body matrix elements parametrized with respect to the neighboring ^{104}Ru, reproduce correctly the $3/2^+$ ground state. The $5/2^+$ member of the multiplet is calculated at 102 keV above the ground state, which is consistent with the 108-keV state in the experimental level scheme and the small spectroscopic factor obtained from the (d, p) reaction. Also, the empirical shell model calculations predict a $9/2^+$ level at 795 keV.

Given that the l-forbidden $M1$ transitions in this mass region are typically hindered by two or three orders of magnitude [20], the extra degrees of forbiddenness observed for the $M1$ transition from the 21-keV, $\nu d_{5/2}$ level is consistent with a more complex structure of the ground state, which could involve a $\nu d_{5/2}^3$ configuration. This scenario could be further tested if we knew the half-life of the 108-keV level, given that the transitions between the same multiplet members are hindered [21]. It worth noting that the $\nu g_{7/2}$ orbit is also observed at low energy, and the occurrence of the respective j^3 multiplet members would make the picture even more complicated. Thus, to account for all single-particle orbits, detailed shell-model calculations are needed.

An alternative approach to the problem would be to restrict the valence space as it is realized in the particle-core coupling models. In the weak-coupling model [22], discussed in the literature as a possible approach to the ^{105}Ru case, the excitations of an odd-mass nucleus are considered to be either single-particle or collective excitations of the even-even core. In this model, the $M1$ transitions between the same multiplet members are forbidden while the $E2$ transitions are enhanced. This resembles the ^{105}Ru case; however, the magnitude of the multiplets splitting in ^{105}Ru is of the order of the first phonon energy, which makes it difficult to identify the multiplet members. Also, the weak coupling model, which should work better for less deformed nuclei, fails in describing ^{101}Ru [23], suggesting that it might not be suitable for ^{105}Ru too.

In the present work, the particle-core coupling concept will be further tested for ^{105}Ru by using the rigid-triaxial-rotor-plus-particle model (RTRPM) [24]. This model seems to be appropriate for the case of ^{105}Ru, given that the nucleus is located in an island of triaxal nuclei.

A. Rigid-triaxial-rotor-plus-particle model calculations

Theoretical calculations for ^{105}Ru were performed with the RTRPM in a strong coupling basis [24]. The single-particle wave functions were calculated with GAMPN code, which is part of the ASYRMO package [25]. A standard set of the Nilsson parameters [26] $\kappa_4 = 0.070$, $\mu_4 = 0.39$, $\kappa_5 = 0.062$, and $\mu_5 = 0.43$ was used. The level energies were calculated with ASYRMO [25], which diagonalyzes the particle+triaxial-rotor Hamiltonian. The quadrupole deformation ϵ_2 and the moment-of-inertia $\hbar^2/2\Im = E_{2^+}/6$ parameters were deduced from the neighboring even-even nuclei. A Corriolis attenuation factor $\xi = 0.7$ was also used to obtain a better description of the band structure. The pairing was parametrized via GN0 = 22.0, GN1 = 8.0 and IPAIR = 5.0. In order to obtain a better fit to the experimental data, ϵ_2, ϵ_4, γ, and E_{2^+} parameters were varied. A good fit to the experimental level energies

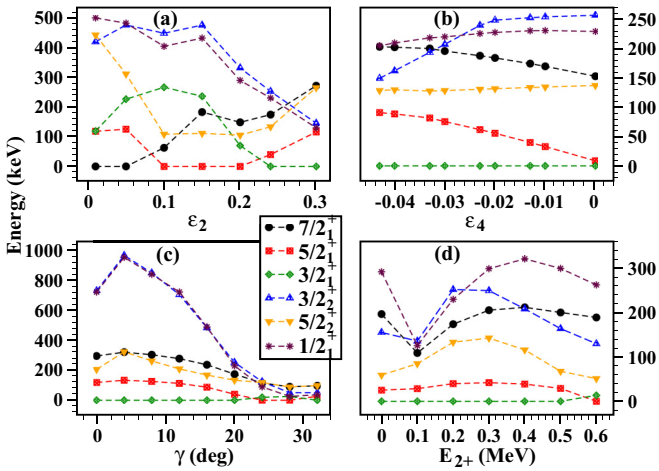

FIG. 4. (Color online) Evolution of the low-lying positive-parity states in ^{105}Ru as a function of the rigid-triaxial-rotor-plus-particle model parameters (a) ϵ_2, (b) ϵ_4, (c) γ, and (d) E_{2^+}. In each subfigure, the unfitted parameters were held fixed to the values given in Fig. 3.

was obtained with $\epsilon_2 = 0.24$, $\epsilon_4 = -0.013$, $\gamma = 20^\circ$, and $E_{2^+} = 0.2$ MeV. This set of parameters is consistent with the respective ϵ_2 and γ, obtained from the neighboring even-even nuclei. A comparison of the experimental and theoretical RTRPM level energies is shown in Fig. 3 and an example of the variation procedures applied for ^{105}Ru is present in Fig. 4.

The level energy dependence on ϵ_2 is shown in Fig. 4(a). The figure shows also that $3/2^+$ is the ground state in ^{105}Ru only at large deformations, i.e., $\epsilon \geqslant 0.24$. Also, the relative position of the low-lying states strongly depends on the deformation parameter ϵ_2.

Figure 4(b) shows that $3/2^+$ is the ground state of ^{105}Ru in a wide range of ϵ_4. This parameter slightly affects also the behavior of the $1/2^+_1$ and $5/2^+_2$ levels, while its influence on the $3/2^+_2$, $5/2^+_1$ and $7/2^+_1$ level energies is stronger.

Figure 4(c) shows that the ^{105}Ru level energies strongly depend on the parameter of triaxial deformation γ for $5^\circ \leqslant \gamma \leqslant 25^\circ$. This is well pronounced for the $1/2^+_1$ and $5/2^+_2$ levels and to a lower extent for the $7/2^+_1$, $5/2^+_1$ and $3/2^+_1$ levels. Except for $\gamma = 24^\circ$ to 26°, $3/2^+$ is the ground state in the entire range of $0^\circ \leqslant \gamma \leqslant 30^\circ$.

Figure 4(d) shows that the ground state is less sensitive to the moment-of-inertia parameter, and $3/2^+$ is the ground state for $E_{2^+} < 0.6$ MeV. Depending on the effect of the moment-of-inertia parameter on the level energies, two subsets of states can be distinguished. The first group of levels is formed by the $3/2^+_1$ and $5/2^+_1$ levels, which are almost independent on this parameter. The second subset is formed by the $1/2^+$ and the $7/2^+$ states with energies strongly dependent on the moment-of-inertia parameter. $3/2^+_2$ and $5/2^+_2$ have a more intermediate trend with respect to the E_{2^+} parameter.

As shown in Fig. 3, a good overall description of the experimental bands, based on the $7/2^+$ and $5/2^+_1$ excited states, is achieved up to $19/2^+$. At higher spins, the experimental bands are more squeezed than the theoretical. This effect could be explained by the backbending usually observed in the positive parity bands of the odd-N, even-Z nuclei in this mass region. Indeed, the positive-parity sequence, based on the $7/2^+$ state, closely resembles the yrast band in ^{104}Ru, as shown in Fig. 3, where backbending is observed.

The energy of the non-yrast $5/2^+_2$ and $1/2^+$ states, experimentally observed close to the ground state, is also well reproduced. The only major discrepancy between the theory and the experiment at low energies is in the $3/2^+_2$ level energy, which is underestimated by the calculations by approximately 200 keV. This is somewhat surprising, given this level is expected to be of single-particle nature and hence should be in the model space.

The $M1$ and $E2$ transition probabilities were calculated with PROBAMO [25]. The standard value of GSFAC = 0.60 for the modification of the free gyromagnetic factor was used. The magnetic moment of the $3/2^+$ ground state, obtained from the RTRPM calculations is $\mu = -0.13\mu_N$, which is consistent with the experimental value $\mu = (-)0.32(+8-20)\mu_N$ [27].

The $B(E2) = 20$ W.u., calculated for the $5/2^+_1 \rightarrow 3/2^+_1$ isomeric transition, is consistent with the experimental value 30.7 W.u., and shows that the $5/2^+_1$ wave function has a collective component. However, the $B(M1) = 0.010$ W.u., calculated with RTRPM, is highly overestimated given that the experimental $B(M1) = 3 \times 10^{-4}$ W.u. Even though the theoretical $B(M1)$ is enhanced with respect to the experimental value, this is still consistent with the experimental data. In the case where the initial state is a $\nu d_{5/2}$ state and the ground state involves a $\nu d^3_{5/2}$ component, which is outside the RTRPM model space, extra degrees of forbiddenness can be expected.

The 55-ns isomer, observed at 164-keV in ^{105}Ru [17] has an even more obscure structure. This is partially because the existing experimental data does not allow a specific J^π assignment to that level [17], and also the $T_{1/2} = 55$ ns was assigned to a $1/2^+$ level [28] rather than to the 164-keV level, assuming the 143-keV transition is an l-forbidden transition. Indeed, the RTRPM calculations does predict a $3/2^+$ state at 251 keV, which could be the 164-keV state in Ref. [17]; however, it decays to the first and the second $5/2^+$ states via transitions with $B(M1) = 2 \times 10^{-3}$ W.u. and 3.3×10^{-2} W.u., respectively. The extra degree of hindrance, observed in the experimental $B(M1)$ to the $5/2^+_2$ state, could be related to the structure of the final state given that it is a member of the $\nu d^3_{5/2}$ multiplet. Similarly, the $B(M1) = 0.03 \times 10^{-2}$ W.u. decay branch to the ground state, calculated with the RTRPM, is not experimentally observed. Hence, to completely understand the structure of the 164-keV state more experimental data are needed, including unambiguous data for the J^π assignments and a thorough study of its decay branches.

IV. CONCLUSIONS

^{105}Ru was produced in induced fission reaction. Its level scheme was extended up to $27/2^+$ and a new positive-parity band was identified. Rigid-triaxial-rotor-plus-particle model calculations were performed for ^{105}Ru. The model was parametrized to fit the level energies, known from literature, as well as the data obtained in the present study. In the medium-spin regime, i.e., for $J^\pi \leqslant 19/2^+$, the model

correctly describes the level energies. At higher spins, the experimental level energies are overestimated by the model calculations. This is not surprising, since the positive-parity bands in the odd-mass, even-Z nuclei from this mass region exhibit a backbending due to a $vh_{11/2}$ pair breaking, which is outside the RTRPM model space. The model fails in describing the hindrance of the isomeric $M1$ transitions to the ground state also, which is attributed to the structure of the final state. These features show the complexity of the low-energy part of the ^{105}Ru spectrum, where single-particle orbits, three-particle clusters, and collectivity compete.

ACKNOWLEDGMENTS

This work is supported by the Bulgarian National Science fund under Contract No. DMU02/1 and the German BMBF under Contract No. 06 BN 109.

[1] J. Blachot, Nucl. Data Sheets. **108**, 2035 (2007).
[2] S. Lalkovski *et al.*, J. Phys.: Conf. Ser. **366**, 012029 (2012).
[3] D. Kameda *et al.*, Phys. Rev. C **86**, 054319 (2012).
[4] P.-A. Söderström *et al.*, Phys. Rev. C **88**, 024301 (2013).
[5] K. Sümmerer, N. Kaffrell, and N. Trautmann, Z. Phys. A **273**, 77 (1975).
[6] H. T. Fortune, G. C. Morrison, J. A. Nolen, and P. Kienle, Phys. Rev. C **3**, 337 (1971).
[7] P. Maier-Komor, P. Glässel, E. Huenges, H. Rösler, H. J. Scheerer, H. K. Vonach, and H. Baier, Z. Phys. A **278**, 327 (1976).
[8] B. Hrastnik, H. Seyfrath, A. M. Hassan, W. Delang, and P. Gottel, Nucl. Phys. A **219**, 381 (1974).
[9] H. H. Güven, B. Kardon, and H. Seyfrath, Z. Phys. A **287**, 271 (1978).
[10] N. Fotiades *et al.*, Phys. Rev. C **58**, 1997 (1998).
[11] D. C. Radford, Nucl. Instrum. Methods A **361**, 297 (1995).
[12] T. Kutsarova *et al.*, Phys. Rev. C **79**, 014315 (2009).
[13] S. Lalkovski *et al.*, Phys. Rev. C **75**, 014314 (2007).
[14] E. A. Stefanova *et al.*, Phys. Rev. C **86**, 044302 (2012).
[15] E. A. Stefanova *et al.*, Phys. Rev. C **63**, 064315 (2001).
[16] E. A. Stefanova *et al.*, Phys. Rev. C **62**, 054314 (2000).
[17] D. De Frenne and E. Jacobs, Nucl. Data Sheets **105**, 775 (2005).
[18] T. Kibédi, T. W. Burrows, M. B. Trzhaskovskaya, P. M. Davidson, and C. W. Nestor, Jr., Nucl. Instrum. Methods A **589**, 202 (2008).
[19] K. Heyde, *The Nuclear Shell Model* (Springer-Verlag, Berlin, 1994).
[20] W. Andrejtscheff, L. K. Kostov, L. G. Kostova, P. Petkov, M. Senba, N. Tsoupas, Z. Z. Ding, and C. Tuniz, Nucl. Phys. A **445**, 515 (1985).
[21] A. de-Shalit and I. Talmi, *Nuclear Shell Theory, Pure and Applied Physics* Vol. 14 (Academic, New York, 1963).
[22] A. de Shalit, Phys. Rev. **122**, 1530 (1961).
[23] A. Goswami and D. K. McDaniels, Phys. Rev. C **7**, 1263 (1973).
[24] S. E. Larsson, G. Leander, and I. Ragnarsson, Nucl. Phys. A **307**, 189 (1978).
[25] P. Semmes and I. Ragnarsson, The Particle + Triaxial Rotor Model: A User's Guide, presented at the Risö Hands-On Nuclear Structure Theory Workshop, June 1992 (unpublished).
[26] T. Bengtsson and I. Ragnarsson, Nucl. Phys. A **436**, 14 (1985).
[27] E. Hagn, J. Wese, and G. Eska, Z. Phys. A **299**, 353 (1981).
[28] R. E. Holland, F. J. Lynch, and B. D. Belt, Phys. Rev. C **17**, 2076 (1978).